

Ferroelectricity of pristine $Hf_{0.5}Zr_{0.5}O_2$ films fabricatedby atomic layer deposition

Luqiu Chen(陈璐秋), Xiaoxu Zhang(张晓旭), Guangdi Feng(冯光迪), Yifei Liu(刘逸飞), Shenglan Hao(郝胜兰), Qiuxiang Zhu(朱秋香), Xiaoyu Feng(冯晓钰), Ke Qu(屈可), Zhenzhong Yang(杨振中), Yuanshen Qi(祁原深), Yachin Ivry, Brahim Dkhil, Bobo Tian(田博博), Junhao Chu(褚君浩), and Chungang Duan(段纯刚)
Citation: Chin. Phys. B, 2023, 32 (**10**): 108102. DOI: 10.1088/1674-1056/accff3
Journal homepage: http://cpb.iphy.ac.cn; http://iopscience.iop.org/cpb

What follows is a list of articles you may be interested in

A new transition metal diphosphide α-MoP_2 synthesized by a high-temperature and high-pressure technique

Xiaolei Liu(刘晓磊), Zhenhai Yu(于振海), Jianfu Li(李建福), Zhenzhen Xu(徐真真), Chunyin Zhou(周春银), Zhaohui Dong(董朝辉), Lili Zhang(张丽丽), Xia Wang(王霞), Na Yu(余娜), Zhiqiang Zou(邹志强),Xiaoli Wang(王晓丽), and Yanfeng Guo(郭艳峰)
Chin. Phys. B, 2023, 32 (**1**): 018102. DOI: 10.1088/1674-1056/ac633d

Photon-interactions with perovskite oxides

Hongbao Yao(姚洪宝), Er-Jia Guo(郭尔佳), Chen Ge(葛琛), Can Wang(王灿), Guozhen Yang(杨国桢), and Kuijuan Jin(金奎娟)
Chin. Phys. B, 2022, 31 (**8**): 088106. DOI: 10.1088/1674-1056/ac754c

Stability and optoelectronic property of lead-free halide double perovskite $Cs_2B'BiI_6$ (*B*' = Li, Na and K)

Yunhui Liu(刘云辉), Wei Wang(王威), Feng Xiao(肖峰), Liangbin Xiong(熊良斌), and Xing Ming(明星)
Chin. Phys. B, 2021, 30 (**10**): 108102. DOI: 10.1088/1674-1056/ac05a5

Effects of Ni doping on the structural properties and collapse of magnetic ordering in $NdFe_{1-x}Ni_xO_3$ ($0.1 \le x \le 0.7$) orthoferrites

I. Ahmad, M. J. Akhtar, M. Siddique
Chin. Phys. B, 2016, 25 (**2**): 028101. DOI: 10.1088/1674-1056/25/2/028101

Morphology-controlled synthesis of $SrTiO_3$ micro-scale particles

Cao Jia-Feng (曹加锋), Ji Yue-Xia (冀月霞)
Chin. Phys. B, 2014, 23 (**12**): 128104. DOI: 10.1088/1674-1056/23/12/128104

Ferroelectricity of pristine $Hf_{0.5}Zr_{0.5}O_2$ films fabricated by atomic layer deposition

Luqiu Chen(陈璐秋)[1,2,†], Xiaoxu Zhang(张晓旭)[1,2,†], Guangdi Feng(冯光迪)[1,2], Yifei Liu(刘逸飞)[1], Shenglan Hao(郝胜兰)[1], Qiuxiang Zhu(朱秋香)[1,2,3,‡], Xiaoyu Feng(冯晓钰)[1], Ke Qu(屈可)[1], Zhenzhong Yang(杨振中)[1,§], Yuanshen Qi(祁原深)[4], Yachin Ivry[5], Brahim Dkhil[6], Bobo Tian(田博博)[1,2,¶], Junhao Chu(褚君浩)[1,7,8], and Chungang Duan(段纯刚)[1,9]

[1] *Key Laboratory of Polar Materials and Devices (MOE), Ministry of Education, Shanghai Center of Brain-inspired Intelligent Materials and Devices, Department of Electronics, East China Normal University, Shanghai* 200241, *China*

[2] *Zhejiang Laboratory, Hangzhou* 310000, *China*

[3] *Guangdong Provisional Key Laboratory of Functional Oxide Materials and Devices, Southern University of Science and Technology, Shenzhen* 518055, *China*

[4] *Department of Materials Sciences and Engineering, Guangdong Technion-Israel Institute of Technology, Shantou* 515063, *China*

[5] *Department of Materials Science and Engineering, Solid-State Institute, Technion-Israel Institute of Technology, Haifa* 3200003, *Israel*

[6] *Université Paris-Saclay, CentraleSupélec, CNRS-UMR*8580, *Laboratoire Structures, Propriétés et Modélisation des Solides, Gif-sur-Yvette* 91190, *France*

[7] *State Key Laboratory of Infrared Physics, Shanghai Institute of Technical Physics, Chinese Academy of Sciences, Shanghai* 200083, *China*

[8] *Institute of Optoelectronics, Fudan University, Shanghai* 200433, *China*

[9] *Collaborative Innovation Center of Extreme Optics, Shanxi University, Shanxi* 030006, *China*

(Received 25 March 2023; revised manuscript received 22 April 2023; accepted manuscript online 25 April 2023)

Hafnium-based ferroelectric films, remaining their ferroelectricity down to nanoscale thickness, present a promising application for low-power logic devices and nonvolatile memories. It has been appealing for researchers to reduce the required temperature to obtain the ferroelectric phase in hafnium-based ferroelectric films for applications such as flexible and wearable electronics. This work demonstrates that a remanent polarization (P_r) value of > 5 μC/cm^2 can be obtained in as-deposited $Hf_{0.5}Zr_{0.5}O_2$ (HZO) films that are fabricated by thermal atomic layer deposition (TALD) under low temperature of 250 °C. The ferroelectric orthorhombic phase (o-phase) in the as-deposited HZO films is detected by scanning transmission electron microscopy (STEM). This low fabrication temperature further extends the compatibility of ferroelectric HZO films to flexible electronics and avoids the cost imposed by following high-temperature annealing treatments.

Keywords: $Hf_{0.5}Zr_{0.5}O_2$ (HZO), ferroelectric, orthorhombic, without annealing

PACS: 81.05.–t, 77.80.–e, 77.55.fp, 85.50.–n **DOI:** 10.1088/1674-1056/accff3

1. Introduction

Storage technologies are approaching physical limits with the continuous reduction of semiconductor process nodes. It is thus urgent to explore new materials and technologies to promote the development of higher density, lower power consumption and faster memory devices. Among new types of memory technologies, ferroelectric-based memory devices demonstrate appealing potential because of their low-writing power, fast-switching speed and high endurance.[1–3] However, traditional perovskite-based (ABO_3) ferroelectric materials, like Pb(Zr, Ti)O_3 (PZT) and $BaTiO_3$ (BTO) have difficulty in maintaining ferroelectricity at the nanometer scale. It results in ferroelectric random access memory stagnating at 130 nm node.[4–6] The discovery of unprecedented ferroelectric properties in Si-doped HfO_2 thin films with a fluorite structure in 2011 quickly piqued intensive attention on HfO_2-based ferroelectrics in both academic and industrial communities.[7] In contrast to the perovskite counterparts, HfO_2-based ferroelectric films not only can maintain ferroelectricity within ten nanometers but also are compatible with common Si-based complementary metal–oxide–semiconductor (CMOS) processing methods. These merits break the traditional ferroelectric memory's bottleneck and make HfO_2-based ferroelectric films promising for next-generation electronics.

Various fabrication methods have been explored for HfO_2-based ferroelectric films over the last decade, including atomic layer deposition (ALD), sputtering,[8–10] pulsed laser deposition (PLD),[11] and chemical solution deposition.[12–14] Among them, ALD stands out as the most established deposition technique for controlling thickness at the atomic level and producing large-scale homogenous films. It is generally accepted that the ferroelectricity of doped HfO_2-based films comes from the metastable non-centrosymmetric o-phase that exhibits the $Pca2_1$ space group. To obtain the metastable fer-

[†]These authors contributed equally to this work.
[‡]Corresponding author. E-mail: qxzhu@clpm.ecnu.edu.cn
[§]Corresponding author. E-mail: zzyang@phy.ecnu.edu.cn
[¶]Corresponding author. E-mail: bbtian@ee.ecnu.edu.cn

© 2023 Chinese Physical Society and IOP Publishing Ltd

roelectric o-phase, ALD-grown films typically require high-temperature annealing.[15,16] Among various dopants, such as Zr,[16–19] Al,[20–22] Si,[23,24] La,[25,26] annealing temperature for Zr-doped HfO_2 films is relatively low.[27]

Due to the limitations of large-scale integrated circuits, fabrication temperature is typically restricted to lower temperatures. Therefore, decreasing annealing temperature is of both scientific and technological interest. Using different methods to improve ferroelectricity at low processing temperatures, could be attributed to increasing the o-phase in the film. Elaborate control on experimental parameters, including annealing period, annealing velocity, and pressure, was put forward to tackle this challenge. For instance, by increasing the pressure to 50 atm during annealing, Kim *et al.* obtained ferroelectric HZO films at a reduced annealing temperature of 450 °C.[28] Lehninger *et al.* prolonged the annealing time to 2 h and reported ferroelectric HZO films under 400 °C post-thermal processing.[29] The transition from non-ferroelectric tetragonal phase (t-phase) to o-phase under either high pressure or time-extended annealing process accounts for the ferroelectricity in their HZO films. Despite of these inspiring progresses, ferroelectricity acquired under much low temperature processing is still appealing, especially for applications in flexible and wearable electronics. Yu *et al.* grew 30 nm HZO thin films on flexible substrates and annealed them at 380 °C for 120 s.[30] The low thermal conductivity and thermal expansion coefficient of plastic substrate make it possible to enhance the ferroelectric phase ratio of HZO films by optimizing the annealing rate and film thickness. Persson *et al.* deposited HZO films on high-mobility InAs semiconductor and decreased the annealing temperature down to 370 °C.[31] Takashi Onaya *et al.* reported 10 nm $Hf_{0.43}Zr_{0.57}O_2$ films annealed at 300 °C for 60 s, and proposed that nanocrystals with metastable o/t/cubic phases in the as-deposited Zr-doped HfO_2 films may serve as nuclei sites for ferroelectric phase during annealing process, because plasma-enhanced ALD has stronger oxidizing power than TALD.[32]

Although ferroelectric Zr-doped HfO_2 films have been reported under 400 °C thermal processing, the annealing process is still indispensable for enhanced ferroelectric o-phase.[33] With the elimination of the annealing process, ferroelectric $Hf_{0.34}Zr_{0.66}O_2$ films were obtained by Kim *et al.* using cyclopentadienyl-based precursors growth,[17] while Qi *et al.* prepared ferroelectric HZO films by adding a TiO_2 interfacial layer between HZO and TiN at 300 °C.[34] These works used either stable precursors or a dielectric layer to trigger the formation of ferroelectric o-phase. Further experiments are still required to directly form the ferroelectric o-phase without extra experimental processing.

Herein, we demonstrate a record low fabrication temperature of 250 °C for ferroelectric HZO films without needing a post-annealing process. Grazing-angle incidence x-ray diffraction (GIXRD) measurement and Cs-corrected annular-dark-field (ADF) STEM are used to confirm the existence of ferroelectric o-phase in as-deposited HZO films. Polarization versus electric field (*P*–*E*) hysteresis loops in the TiN/as-deposited HZO/TiN capacitor further confirm the ferroelectricity. The endurance is up to $\sim 10^7$ cycles. This finding enables a further decrease of the fabrication temperature for HfO_2-based ferroelectric films and avoids undesirable chemical reactions during annealing, offering a new pathway for low-temperature flexible and wearable electronics based on HZO devices.

2. Experimental methods

For metal–ferroelectric–metal (MFM) capacitors, 5 nm-thick TiN films are deposited on heavily n-doped Si substrates via magnetron sputtering at room temperature to form the bottom electrode. Subsequently, 15 nm thick HZO films are grown by TALD at 250 °C, using Tetrakis(dimethylamino)hafnium (TDMA-Hf) and Tetrakis(dimethylamino)zirconium (TDMA-Zr) as precursors, and H_2O as an oxygen source. The cycle ratio between HfO_2 and ZrO_2 is 1:1. After ALD deposition, capacitors are prepared by photolithography to obtain 100 μm × 100 μm top electrodes. A 50 nm TiN is deposited on the HZO films via magnetron sputtering, followed by photolithography patterning. Besides, several reference capacitors are crystallized by rapid thermal annealing (RTA) with temperatures ranging from 150 °C to 750 °C in ambient N_2 for 30 s.

The crystallinity of HZO thin films is investigated via GIXRD using Cu-$K\alpha$ radiation ($\lambda = 1.5405$ Å) with an incidence angle of 0.5°. The thickness of HZO films is obtained by x-ray reflectivity (XRR). ADF-STEM images are performed to characterize the capacitors in more detail. *P*–*E* measurements and endurance tests are performed at room temperature using a ferroelectric analyzer (TF Analyzer 3000) at 1 kHz/5 V and 10 kHz/4.5 V, respectively.

3. Results and discussion

The ferroelectricity of the HZO films is explored in MFM capacitors (Fig. 1(a)). Figure 1(b) shows the cross-sectional HAADF-STEM image of a TiN/HZO/TiN/SiO_2/Si stack, which confirms 15 nm thickness of as-deposited HZO film. The crystallinity and phase identification are investigated by GIXRD measurements. Figure 1(c) displays the GIXRD pattern of as-deposited MFM capacitor. The o (111)/t (011) at ∼ 30.5°, o (002)/t (110) at ∼ 35.3°, and o (022)/t (020) at ∼ 50.8° diffraction peaks of HZO, and TiN (111) at ∼ 37.2°

reflection can be identified.[35] Therefore, as-deposited HZO film has a polycrystalline structure composed of t-phase and o-phase.

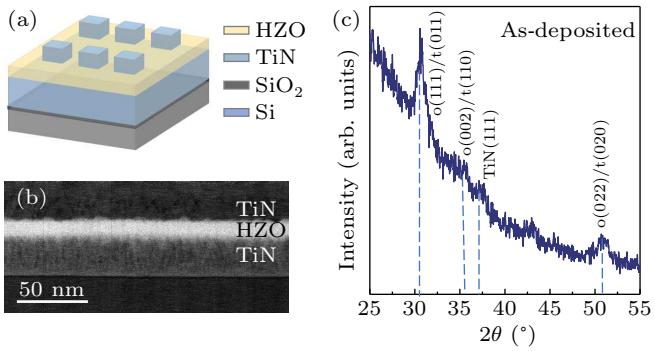


Fig. 1. (a) Schematics of the MFM capacitors: TiN (50 nm)/HZO (15 nm)/TiN (50 nm)/SiO_2/Si. (b) ADF-STEM image of MFM capacitor. (c) GIXRD patterns of as-deposited MFM capacitors.

To confirm the o-phase grain in asdeposited HZO film, we perform Cs-corrected STEM imaging for atomic characterization. As shown in Fig. 2, cross-section ADF-STEM images exhibit TiN/HZO/TiN stack with an o-phase grain. Zooming into the dashed yellow square in Fig. 2(a), the lattice spacings of 2.35 Å/2.7 Å (Fig. 2(b)) reveal that the o-phase grain possesses $Pbc2_1$ symmetry, which is considered as the origin of ferroelectricity in hafnium-based materials. HAADF-STEM image is taken along the [001] direction and corresponding crystal structure of HZO is shown in Fig. 2(c). This result indicates that an o-phase grain could be formed without additional annealing.

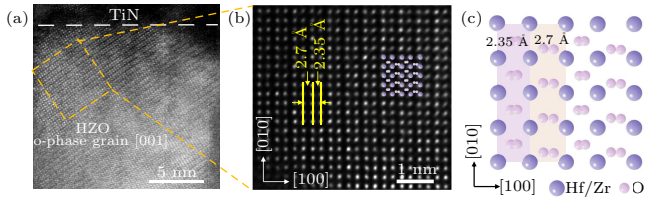


Fig. 2. (a) Cross-section ADF-STEM image of TiN/HZO/TiN stack, showing an o-phase [001] grain. (b) HAADF-STEM image acquired from the dashed yellow square area in panel (a), demonstrating the $Pbc2_1$ phase structure. (c) Crystal structure of HZO viewed along [001] direction.

Electrical tests are performed to further confirm the ferroelectricity of asdeposited HZO films. It is also worth noting that, for as-deposited HZO films, the *P*–*E* curve shows a distinct ferroelectric hysteresis. Figure 3(a) shows *P*–*E* hysteresis loops gradually open along the grey line direction with increasing measuring cycles. Remarkably, the P_r value of as-deposited HZO films increases significantly as the measuring cycles increase, which becomes quasi-stable with a value of ~ 5 μC/cm^2 after $\sim 10^3$ cycles and reaches 5.7 μC/cm^2 after $\sim 10^7$ cycles. The gradually increased P_r value implies transitioning from t-phase to o-phase during measuring cycles.[36–38] It is worth noting that ferroelectricity survives $\sim 10^7$ cycles for as-deposited HZO films.

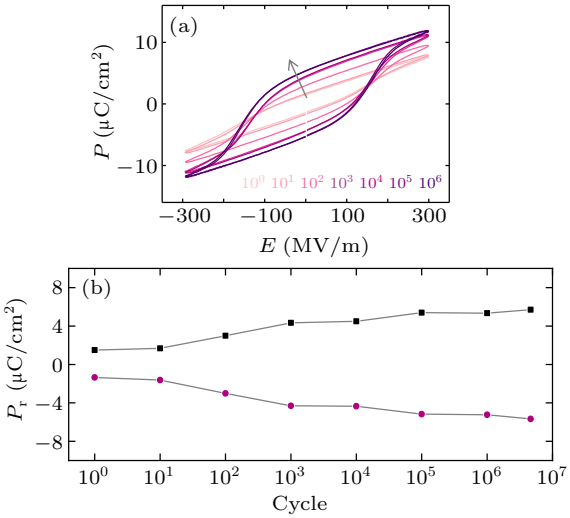


Fig. 3. (a) Endurance test results of as-deposited TiN/HZO/TiN capacitors. (b) P_r values are extracted from panel (a) as functions of the number of switching cycles.

As a comparison, other HZO films suffering post-RTA treatments at temperatures ranging from 150 °C to 750 °C are also checked. Figures 4(a) and 4(b) show *P*–*E* curves and corresponding *I*–*E* curves obtained under 1 kHz conditions. Electric field cycling with 10^3 cycles at 4 V and 5 kHz is preperformed to keep HZO films free of the wake-up effect.[39–42] The hysteresis loops are poor for films after RTA treatment at temperatures between 150 °C and 350 °C. With increasing RTA temperatures from 450 °C to 650 °C, the films show enhanced ferroelectricity with a maximum $2P_r$ of ~ 32 μC/cm^2 at 650 °C. Further increasing RTA temperature up to 750 °C, leakage current becomes noticeable. The P_r value obtained from *P*–*E* curves is presented in Fig. 4(d). To understand the difference in P_r value among HZO films, GIXRD spectrum, especially in the 2θ range of 29°–32.2°, is analyzed, which can give information about the relative proportion of o-phase and t-phase in HZO films.[16,24,43] As shown in Fig. 4(c), the fitting of GIXRD patterns by Gaussian–Lorentzian cross product function, with fixed peak positions at 30.4° and 30.8° for o (111) and t (011) respectively, can be used to obtain the o/t phase proportion.[35] The relative proportion of o/t derived from GIXRD fittings is presented in Fig. 4(e). Notably, the P_r value (Fig. 4(d)) accords well with the proportion of o/t (Fig. 4(e)), supporting that the change of ferroelectricity in our ALD-fabricated HZO films originates from the change of o-phase proportion. Temperature dependences of P_r value (Fig. 4(d)) and proportion of o/t (Fig. 4(e)) imply that annealing at a low temperature < 400 °C does not effectively contribute to the crystallization of ferroelectric o-phase.

Figure 5 summarizes a comparison of the P_r value obtained from this work and other reported HfO_2-based ferroelectric films. Our work reports the ferroelectricity of HZO films by competitive low temperature processing.

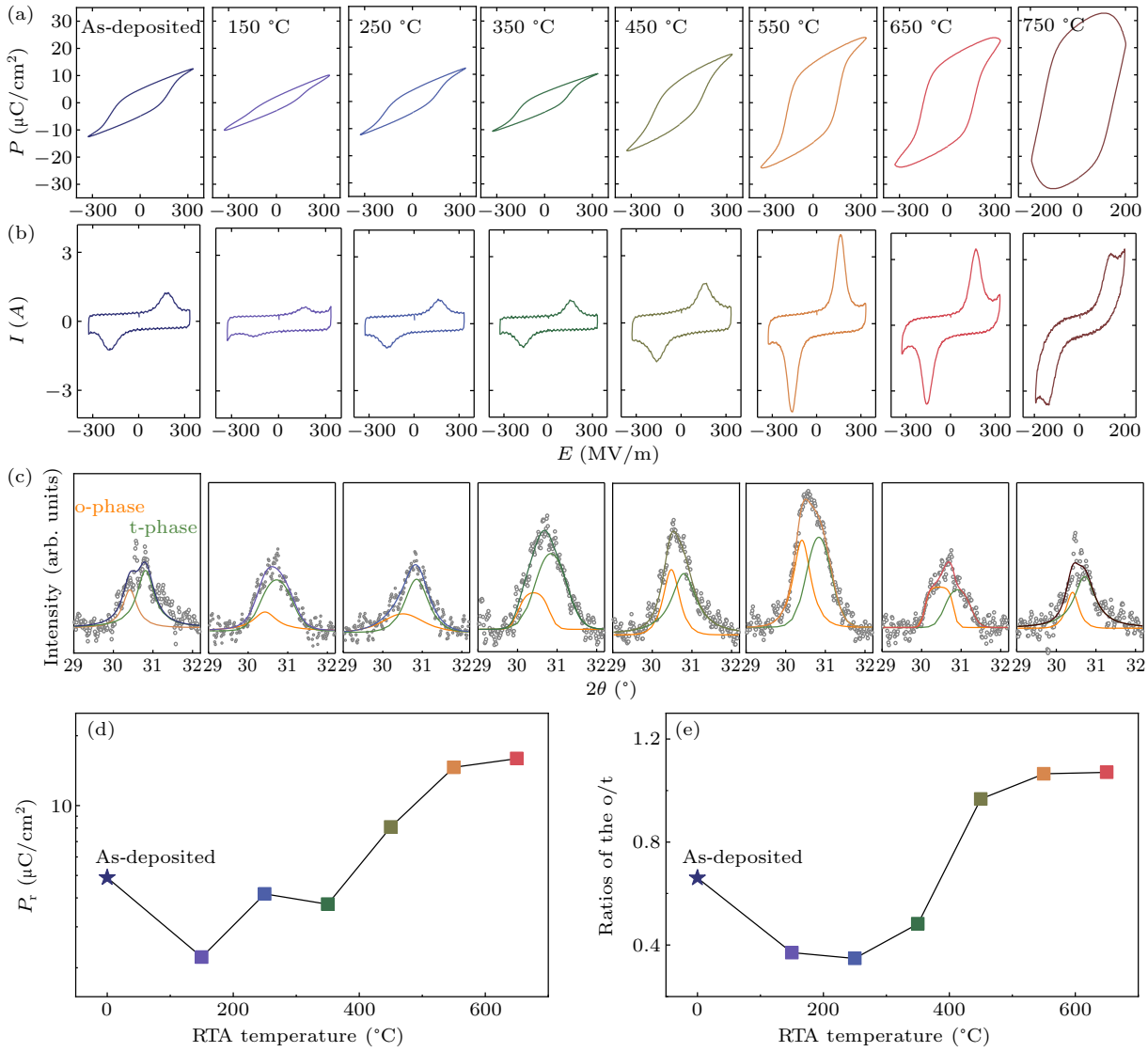


Fig. 4. (a) *P*–*E* hysteresis curves and (b) *I*–*E* curves of TiN/HZO/TiN capacitors with different RTA conditions at 1 kHz/5 V. (c) Ratios of the o-phase/t-phase (o/t) for HZO films as-deposited and under different RTA treatment, by fitting the peak at 30°–31° from GIXRD pattern. The orange and green curves are fittings for the o-phase and the t-phase, respectively. (d) P_r and (e) ratios of the o/t for HZO films as a function of RTA temperature.

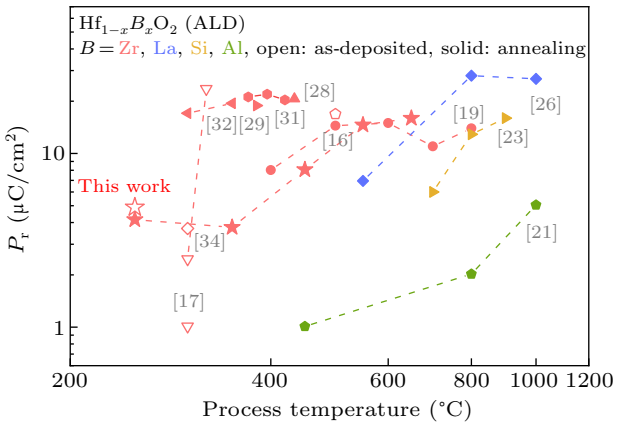


Fig. 5. Comparison of the P_r values of HfO_2-based ferroelectric films that are treated at different temperatures.

4. Conclusion

We demonstrate that ferroelectricity in HZO films can be directly obtained by a low-temperature (as low as 250 °C fabricating temperature) ALD method without any post-annealing process. The as-deposited HZO films show a P_r value of > 5 μC/cm^2 and an endurance of around 10^7 cycles. Atomic resolution ADF-STEM image directly confirms that o-phase grains are formed in as-deposited HZO films. It gives a clue for reducing the processing temperature for ferroelectric HZO films and extending their compatibility for flexible and wearable applications.

Acknowledgments

Project supported by the National Key Research and Development Program of China (Grant No. 2021YFA1200700), the National Natural Science Foundation of China (Grant Nos. T2222025 and 62174053), the Open Research Projects of Zhejiang Laboratory (Grant No. 2021MD0AB03), the Shanghai Science and Technology Innovation Action Plan (Grant Nos. 21JC1402000 and 21520714100), the

Guangdong Provincial Key Laboratory Program (Grant No. 2021B1212040001), and the Fundamental Research Funds for the Central Universities. Yachin Ivry acknowledges support from the Zuckerman STEM Leadership Program as well as from Pazy Research Foundation (Grant No. 149-2020).

References

[1] Niu X, Tian B, Zhu Q, Dkhil B and Duan C 2022 *Appl. Phys. Rev.* **9** 021309

[2] Cui B, Fan Z, Li W, Chen Y, Dong S, Tan Z, Cheng S, Tian B, Tao R, Tian G, Chen D, Hou Z, Qin M, Zeng M, Lu X, Zhou G, Gao X and Liu J M 2022 *Nat. Commun.* **13** 1707

[3] Ma C, Luo Z, Huang W, Zhao L, Chen Q, Lin Y, Liu X, Chen Z, Liu C, Sun H, Jin X, Yin Y and Li X 2020 *Nat. Commun.* **11** 1439

[4] Müller J, Yurchuk E, Schlösser T, Paul J, Hoffmann R, Müller S, Martin D, Slesazeck S, Polakowski P, Sundqvist J, Czernohorsky M, Seidel K, Kücher P, Boschke R, Trentzsch M, Gebauer K, Schröder U and Mikolajick T 2012 *Symposium on VLSI Technology*, June 12–14, 2012, Honolulu, USA, p. 25

[5] Müller J, Böscke T S, Müllera S, *et al.* 2013 *IEEE International Electron Devices Meeting*, December 9–11, 2013, Washington, USA, pp. 10.8.1

[6] Park M H, Lee Y H, Kim H J, Kim Y J, Moon T, Kim K D, Muller J, Kersch A, Schroeder U, Mikolajick T and Hwang C S 2015 *Adv. Mater.* **27** 1811

[7] Böscke T S, Müller J, Bräuhaus D, Schröder U and Böttger U 2011 *Appl. Phys. Lett.* **99** 102903

[8] Kim Y, Woo J, Im S, Lee Y, Kim J H, Im J P, Suh D, Yang S M, Yoon S M and Moon S E 2020 *Curr. Appl. Phys.* **20** 1441

[9] Bouaziz J, Romeo P R, Baboux N and Vilquin B 2019 *ACS Appl. Electron.* **1** 1740

[10] Zhang Y, Xu J, Zhou D, Wang H, Lu W and Choi C 2018 *Chin. Phys. B* **27** 48103

[11] Zhang Z, Hsu S L, Stoica V A, Paik H, Parsonnet E, Qualls A, Wang J, Xie L, Kumari M, Das S, Leng Z, McBriarty M, Proksch R, Gruverman A, Schlom D G, Chen L Q, Salahuddin S, Martin L W and Ramesh R 2021 *Adv. Mater.* **33** 2006089

[12] Starschich S, Griesche D, Schneller T, Waser R and Böttger U 2014 *Appl. Phys. Lett.* **104** 202903

[13] Wei A, Chen C, Tang L, Zhou K and Zhang D 2018 *J. Alloys Compd.* **731** 546

[14] Wang J, Zhou D, Dong W, Yao Y, Sun N, Ali F, Hou X and Liu F 2021 *Adv. Electron. Mater.* **7** 2000585

[15] Sang X, Grimley E D, Schenk T, Schroeder U and LeBeau J M 2015 *Appl. Phys. Lett.* **106** 162905

[16] Muller J, Boscke T S, Schroder U, Mueller S, Brauhaus D, Bottger U, Frey L and Mikolajick T 2012 *Nano Lett.* **12** 4318

[17] Kim H B, Jung M, Oh Y, Lee S W, Suh D and Ahn J H 2021 *Nanoscale* **13** 8524

[18] Park M H, Kim H J, Kim Y J, Lee W, Moon T and Hwang C S 2013 *Appl. Phys. Lett.* **102** 8524

[19] Park M H, Lee Y H, Kim H J, Kim Y J, Moon T, Kim K D, Hyun S D, Mikolajick T, Schroeder U and Hwang C S 2017 *Nanoscale* **10** 716

[20] Florent K, Lavizzari S, Popovici M, Di Piazza L, Celano U, Groeseneken G and Van Houdt J 2017 *J. Appl. Phys.* **121** 204103

[21] Mueller S, Mueller J, Singh A, Riedel S, Sundqvist J, Schroeder U and Mikolajick T 2012 *Adv. Funct. Mater.* **22** 2412

[22] Ma X, Yang H, Xiang J, Wang X, Wang W, Zhang J, Yin H, Zhu H and Zhao C 2017 *Chin. Phys. B* **26** 27701

[23] Lomenzo P D, Takmeel Q, Moghaddam S and Nishida T 2016 *Thin Solid Films* **615** 139

[24] Böscke T S, Teichert S, Bräuhaus D, Müller J, Schröder U, Böttger U and Mikolajick T 2011 *Appl. Phys. Lett.* **99** 112901

[25] Chernikova A G, Kuzmichev D S, Negrov D V, Kozodaev M G, Polyakov S N and Markeev A M 2016 *Appl. Phys. Lett.* **108** 242905

[26] Schroeder U, Richter C, Park M H, Schenk T, Pesic M, Hoffmann M, Fengler F P, Pohl D, Rellinghaus B and Zhou C 2018 *Inorg. Chem.* **57** 2752

[27] Richter C, Schenk T, Park M H, Tscharntke F A, Grimley E D, LeBeau J M, Zhou C, Fancher C M, Jones J L, Mikolajick T and Schroeder U 2017 *Adv. Electron. Mater.* **3** 1700131

[28] Kim T, Park J, Cheong B H and Jeon S 2018 *Appl. Phys. Lett.* **112** 092906

[29] Lehninger D, Olivo R, Ali T, Lederer M, Kämpfe T, Mart C, Biedermann K, Kühnel K, Roy L, Kalkani M and Seidel K 2020 *Phys. Status Solidi (a)* **217** 1900840

[30] Yu H, Chung C C, Shewmon N, Ho S, Carpenter J H, Larrabee R, Sun T, Jones J L, Ade H, O'Connor B T and So F 2017 *Adv. Funct. Mater.* **27** 1700461

[31] Persson A E O, Athle R, Littow P, Persson K M, Svensson J, Borg M and Wernersson L E 2020 *Appl. Phys. Lett.* **116** 062902

[32] Onaya T, Nabatame T, Sawamoto N, Ohi A, Ikeda N, Nagata T and Ogura A 2019 *Microelectron. Eng.* **215** 111013

[33] Chen K Y, Chen P H and Wu Y H 2017 31*st Symposium on VLSI Circuits*, June 5–9, 2017, Kyoto, Japan, p. T84

[34] Qi Y, Xu X, Krylov I and Eizenberg M 2021 *Appl. Phys. Lett.* **118** 032906

[35] Park M H, Kim H J, Kim Y J, Lee W, Moon T and Hwang C S 2013 *Appl. Phys. Lett.* **102** 242905

[36] Fields S S, Smith S W, Ryan P J, Jaszewski S T, Brummel I A, Salanova A, Esteves G, Wolfley S L, Henry M D, Davids P S and Ihlefeld J F 2020 *ACS Appl. Mater. Interfaces* **12** 26577

[37] Kao Y C, Peng H K, Wang Y K, Wu K A, Wang C Y, Lin Y D, Lai T C, Wu Y H, Lin C Y, Hsiao S W, Lee M H and Wu P J 2022 *ACS Appl. Electron. Mater.* **4** 3897

[38] Zheng Y, Zhong C, Zheng Y, Gao Z, Cheng Y, Zhong Q, Liu C, Wang Y, Qi R, Huang R and Lyu H 2021 *Symposium on VLSI Technology*, June 13–19, Kyoto, Japan, p. 1

[39] Pešić M, Fengler F P G, Larcher L, Padovani A, Schenk T, Grimley E D, Sang X, LeBeau J M, Slesazeck S, Schroeder U and Mikolajick T 2016 *Adv. Funct. Mater.* **26** 4601

[40] Zhou D, Xu J, Li Q, Guan Y, Cao F, Dong X, Müller J, Schenk T and Schröder U 2013 *Appl. Phys. Lett.* **103** 192904

[41] Fields S S, Smith S W, Jaszewski S T, Mimura T, Dickie D A, Esteves G, David H M, Wolfley S L, Davids P S and Ihlefeld J F 2021 *J. Appl. Phys.* **130** 134101

[42] Li Y, Zhu H, Li R, Liu J, Xiang J, Xie N, Huang Z, Fang Z, Liu X and Zhou L 2022 *Chin. Phys. B* **31** 88502

[43] Schroeder U, Materano M, Mittmann T, Lomenzo P D, Mikolajick T and Toriumi A 2019 *J. Appl. Phys.* **58** SL0801